Advances in Consumer Research
https://acr-journal.com/
Volume-3 | Issue-2 | Feb 2026
Original Researcher Article

Green route harvesting of hydrogen energy using B-PbBr2 and S-PbBr2 under electrochemical water splitting

Deepa Rosh Tom[1]*, Ajay Majethiya[1]
[1*]Department of Physical Science, V S Patel College of Arts and Science, Bilimora, Veer Narmad South Gujarat University, Surat, 395007, Gujarat, India. *
Email:ID: michaeljintodeepa@gmail.com
[1*]Department of Applied Science and Humanities, School of Engineering, P P Savani University, Kosamba, Surat, 394125, Gujarat, India
Email:ID: ajay.phy@gmail.com

Received: XX
Revised: XX
Accepted: XX
Published: XX

ABSTRACT
For enhanced electrochemical water splitting, to produce clean and green hydrogen, which is the fuel for sustainable energy conversion and storage, high-efficiency and reasonably priced catalysts for the hydrogen evolution reaction (HER) in basic electrolytes are essential. The primary obstacle in green hydrogen is to accomplish continuous and efficient hydrogen evolution at high current densities, which is impossible since prolonged large-current operation quickly degrades the efficiency of hydrogen creation. This work prepared B-$PbBr_2$ and S-$PbBr_2$ nanocomposites using a simple hydrothermal method to improve electrocatalytic green hydrogen production at industrial current densities.
Synthesised B-$PbBr_2$ and S-$PbBr_2$ catalysts exhibit excellent electrochemical water-splitting activity, low overpotential, high current density, and extended stability lasting more than 12 hours. Our work has led to the development of a new electrocatalyst, which is one of the earth-abundant, stable, and highly effective catalysts for water electrolysis. The S-$PbBr_2$/NF electrode significantly enhances conductivity, and its nanosheet structure offers a substantial surface area for catalytic activity. This makes it one of the most promising electrocatalysts for the hydrogen evolution reaction (HER) in an alkaline medium. It's potential is underscored by outstanding stability, excellent catalytic activity and a straightforward production method. The low onset potentials of -0.239 V for S-$PbBr_2$ and -0.242 V for B-$PbBr_2$ further indicate that both electrodes serve as efficient electrocatalysts for HER
Keywords: Water Splitting, Electrochemical Analysis, S doping, B doping, HER

INTRODUCTION:

There has long been interest in hydrogen's potential as a ubiquitous, low-carbon energy source. The prospect of producing hydrogen from various sources, transporting and storing it, and using it to offer final energy services without emissions has been studied by a wide range of experts in recent decades [1]. The two previous major cycles of interest in hydrogen were centred on the use of fuel cells in the transportation industry [2]. Both the breadth of the hydrogen utilisation options under discussion and the degree of international political backing for those options are new. In almost every region, the idea of hydrogen is increasingly coming up in conversations about traditional energy. Many different countries and organisations believe that hydrogen has the potential to play a major and wide-ranging role in the future of the energy sector [3,4].

The green energy problem has emerged as a new challenge of the twenty-first century due to the rapid rise of industrialization, population, and the global economy[5]. The fundamental notion of energy refers to a system's capacity to execute work, but because of its various manifestations, it is challenging to encapsulate it in a singular definition. It is a property of an object that can be altered from one form to another or converted to a different form; however, it cannot be created or annihilated.

There are many diverse energy sources, including sun, wind, hydro, tidal, geothermal, biomass, and hydrogen. Out of all of these sources, hydrogen produces clean energy[6,7]. We are all aware that the world is surrounded by renewable energy sources, particularly water. Water resources are one kind of renewable energy and are abundant and sustainable on the earth. The natural, self-renewing renewable resource, like water, makes an effort to capture energy. It's a self-replenishing attempt to harness energy. Water itself has practical uses, but when it breaks down into hydrogen and oxygen, the industry has designated hydrogen as the next-generation fuel that is ideal for generating electricity, powering cars, and other applications[8,9]. No dangerous gases are emitted into the atmosphere by hydrogen, and it belongs to the category of clean energy sources. As a result of fluctuating oil prices,

a lack of petroleum, and increased awareness of acid rain and air pollution in the 1970s, interest in hydrogen increased[10].

Projections suggest that hydrogen produced from coal or nuclear energy may play a crucial role in long-term energy supply, especially in the transportation sector. As oil and gas supplies increased, oil prices stabilised, opposition to nuclear power increased, and other air pollution control measures were implemented, interest in hydrogen's potential began to decline[11].

Experimental Section:

Preparation of $PbBr_2$, S-$PbBr_2$ and B-$PbBr_2$ nanoparticles: Synthesis of nanoparticles was conducted utilising the chemicals KBr, NH_3, NaOH, Na_2SO_4, $(CH_3COO)_2Pb*3H_2O$ and $Na_2B_4O_5(OH)_4{\cdot}8H_2O$, with tests executed without additional purification. 50 millilitres of distilled water was first introduced into a beaker and agitated for 10 minutes. 2.945 g of lead(II) acetate trihydrate, $(CH_3COO)_2Pb*3H_2O$, was added, and after 5 minutes, 8.1 g of KBr was introduced to the solution, resulting in a colour change to yellow. The pH of the solution has been measured several times every 5 minutes. The pH of the suspension was adjusted to 11 by the progressive addition of 10 ml of ammonia. The solution was subsequently placed in a Teflon-lined autoclave reactor and maintained at 150ºC for 18 hours. The resultant powder was subjected to centrifuging, and the final product was dried at 80ºC for 2 hours. We have extracted the concentrations of $PbBr_2$: S and $PbBr_2$: B from a total yield of 0.5g. For ultrasonication, a concentration such as 85:15 was added to the beaker. The solution was then transferred to an autoclave reactor with a Teflon coating and held at 125°C for 8 h. The resulting powder of S-$PbBr_2$ and B-$PbBr_2$ was cleaned and collected using a centrifuge, and the final product was dried for four hours at 80 degrees.

Fabrication of Working Electrodes: For the fabrication of working electrodes, 0.1 g of the synthesised materials was dispersed in 10 ml of Isopropyl alcohol and sonicated for 30 min. Meanwhile, as purchased, nickel foam was cut into 1.5×1.5 cm^2 and sonicated in 2.5 M HCl for 5 min, which was followed by a wash of distilled water and acetone to remove the impurities present on the surface of Ni foam. After that, the prepared suspension of materials was drop-cast on the Ni foam separately with an active area of 2.25 cm^2. Drop-casted nickel foams were dried for 30 min at 60°C. After that, prepared working electrodes were studied for the hydrogen evolution reaction in the 1 M KOH electrolyte. Figure 1 discusses a step-by-step schematic of the process, detailing the synthesis of the catalyst and the subsequent preparation of electrodes in a systematic manner.

RESULT AND DISCUSSION:

2.1. Material Analysis:

The X-ray diffraction pattern of the $PbBr_2$ sample reveals significant crystallinity (Fig. 1a). The XRD pattern was taken at room temperature between 15º and 90º in the 2θ range. All XRD reflection peaks were indexed using Bragg's law. XRD planes (002), (020), (011), (111), (220), (031), (040), and (232) show the samples' orthorhombic phase structure. All reflection peaks are sharp and shifted in Fig 1b due to S and B doping in pure $PbBr_2$. B-$PbBr_2$ shows a right shift, indicating crystal lattice contraction and reduced interplanar spacing. Scherrer's equation determines powder particle sizes: 12.98 nm, 13.09 nm, and 12.7 nm for $PbBr_2$, S-$PbBr_2$, and B-$PbBr_2$ samples.

The FTIR spectral studies of S-$PbBr_2$ and B-$PbBr_2$ nanocomposites in Fig. 1c, showed the absorption bands from 2353.8 cm^{-1} to 1107 cm^{-1} are typically due to the presence of functional groups like hydroxyl(O-H bending), amine(N-H stretching), carboxyl(C-O stretching)groups, etc. and the region from 987.7 cm^{-1} to 460.3 cm^{-1} is referred as fingerprint region which derives the intra-molecular actions. In Fig. 1d, the PL emission of the $PbBr_2$, S-$PbBr_2$, and B-$PbBr_2$ nanocomposite spectra was observed, and the characteristic emission peaks of the sample were noted at 700.1 nm and 700.4 nm with a band gap of 1.77 eV, respectively, for the doped $PbBr_2$ nanocomposites. Studies say that the excitation wavelength of $PbBr_2$ nanomaterial is between 300nm and 450nm[12]. The doped lead halide perovskites can be directly excited at 700nm due to the unique energy states of S-$PbBr_2$ and B-$PbBr_2$, where the excitation of electrons from the valence band to the conduction band increases, which helps to drive the chemical reactions.

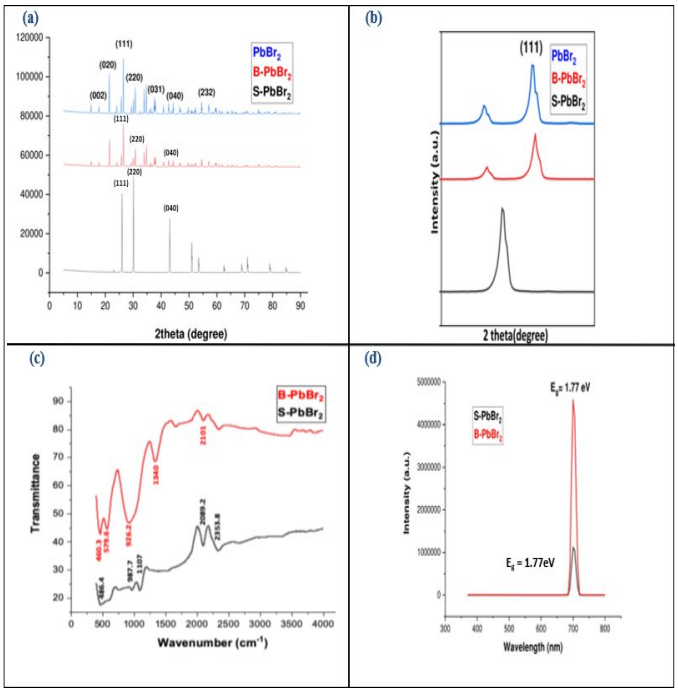

Fig. 1: (a) XRD pattern, (b) Enlarged peak, (c) FTIR and PL spectra of B-$PbBr_2$, S-$PbBr_2$ nano composites

The morphological features of pure and doped $PbBr_2$ nanocomposites were examined by field emission scanning electron microscopy, which is depicted in Figs. 2, 3, and 4. The energy dispersive X-ray spectroscopy (EDAX) was performed and studied for the elemental analysis of prepared $PbBr_2$, S-$PbBr_2$, and B-$PbBr_2$ nanocomposites, as shown in Figs. 2j, 3j, and 4j. The elemental composition of $PbBr_2$ and doped $PbBr_2$ was displayed and showed the uniform distribution of Pb, Br, K, C, and O elements in pure $PbBr_2$ (Figs. 2d-2j). The elements S, Pb, Br, O, and C in S-$PbBr_2$ and the elements B, Pb, Br, O, and C in B-$PbBr_2$ have been identified in EDAX images (Figs. 3d-3j, Figs. 4d-4j). The atomic ratio of Pb, Br, O, and C is 20.4%, 29.6%, 36.2%, and 13.8% in $PbBr_2$. The atomic ratios are like 5.9%, 50.4%, 36%, 0.1%, and 7.5% for the elements C, O, S, Br, and Pb in S-$PbBr_2$, whereas the elements like B, C, O, Br and Pb have the ratio of 0.0%, 10%, 70.1%, 5.5% and 14.4%. FESEM images of $PbBr_2$ have predicted that the sample has a layered structure morphology. The microstructural image of the sample is a nanosheet with a few layers, which is mentioned as the arrow depicted in Fig. 2a. From the SEM micrographs (Figs. 3a-3c), B-$PbBr_2$ has a nanorod morphology of structure, whereas the S-$PbBr_2$ sample has a crystal morphology depicted in Fig. 4a-4c, and after the careful inspection of Fig. 4, it indicates that some of the crystals show a pyramid-like structure. The FESEM image shows nanoparticles with good uniformity and crystallinity.

The atomic ratio of Pb, Br, O, and C is 20.4%, 29.6%, 36.2%, and 13.8% in $PbBr_2$. The X-ray photoelectron spectroscopy of the lead halide nanocomposites was performed, and the survey scan was noted for $PbBr_2$, S-$PbBr_2$, and B-$PbBr_2$ in Fig. 6l. X-ray photoelectron spectroscopy (XPS) was used to identify and study the element valence state and elements in pristine $PbBr_2$, S-$PbBr_2$, and B-$PbBr_2$ samples. This confirms the presence of the Br 3d, C 1s, O 1s, and Pb4f peaks in pure $PbBr_2$ as well as the extra S 2p and B 1s peaks that came from S and B doping in S-$PbBr_2$ and B-$PbBr_2$. The Pb 4f spectra of pristine $PbBr_2$ were displayed in Fig. 6a, where it was revealed that the peaks at binding energies 137.5 eV and 142.4 eV correspond with the Pb4+ binding phases of Pb $4f_{7/2}$ and Pb $4f_{5/2}$, as well as their satellite peaks, which were located at 136 eV and 140.8 eV. The positions of Pb $4f_{7/2}$ and Pb $4f_{5/2}$ of Pb4+ for S-$PbBr_2$ were indicated at 137 eV and 142 eV, as shown in Fig. 6b. Similarly, the positions of Pb $4f_{7/2}$ and Pb $4f_{5/2}$ of Pb4+ for B-$PbBr_2$ were 138 eV and 142.9 eV in Fig. 6c, respectively. The Br 3d spectra of $PbBr_2$ are shown in Fig. 5d, where two Br 3d peaks can be seen at 67.6 eV and 68.5 eV, which correspond to Br $3d_{5/2}$ and Br $3d_{3/2}$. There are two Br 3d peaks for S-$PbBr_2$, situated at 68.5 eV and 75 eV, and for B-$PbBr_2$, the two peaks were present at 67.8 eV and 68.7 eV in Fig. 5e and 5f. In comparison with pure, the peaks of B-$PbBr_2$ were chemically shifted to the right side, and thus the B element draws electron density away from the atoms in the $PbBr_2$, causing a more positive charge and higher binding energy. Similarly, the peaks of S-$PbBr_2$ were chemically shifted to the right side, causing more positive local charges. Fig. 6g-6i displays the deconvolution peaks of the O 1s spectra centred at 528.8 eV and 530.1 eV, respectively, for pure $PbBr_2$, which is attributed to M O bonds, oxygen vacancies, and adsorbed water. The O 1s spectra of S-$PbBr_2$ and B-$PbBr_2$ were obtained at 530 eV, 531 eV, and 535 eV. For the S-$PbBr_2$ sample, the peaks of 2p are seen in Fig. 6j at 160 eV and 168 eV, which are represented by S $2p_3/_2$ and S $2p_1/_2$. At 161 eV and 166 eV, the satellite peaks of S-$PbBr_2$ were located. The binding energy at 190.8 eV drew attention to the peak 1s with a satellite peak of 188 eV for the sample B-$PbBr_2$ depicted in Fig. 6k. Catalytic activity can be increased through S and B-doping by altering the electrical structure and generating more active sites.

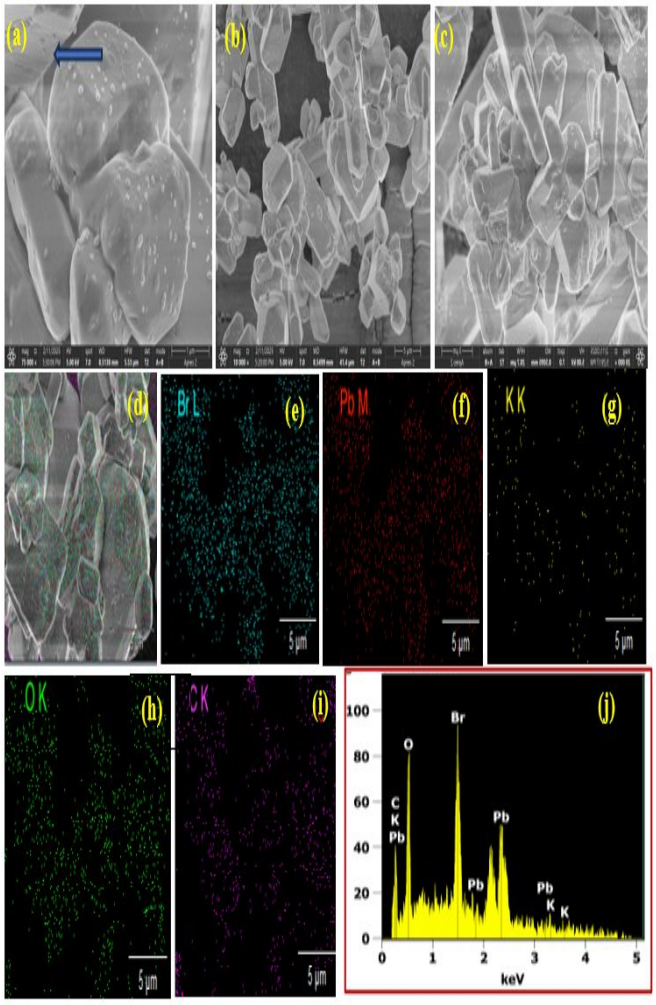

Fig. 2: (a) SEM images of $PbBr_2$ at 1 µm, (b) 3 mm, (c) 5mm, (d) elemental mapping of PbBr2, (e) Br, (f) Pb, (g) K, (h) O,(i) elements, (j) EDAX analysis.

2.2. Study of Electrochemical Hydrogen Evolution Reaction:

A conventional three-electrode potentiostat system and electrochemical workstation, Auto lab/PGSTAT-M204, in alkaline media (1 M KOH), were used to examine the electrochemical measurements for the

hydrogen evolution reaction of $PbBr_2$ and $PbBr_2$: S, $PbBr_2$: B electrodes of Nickel Form(NF). The $PbBr_2$, $PbBr_2$: S and $PbBr_2$: B electrodes worked as a working electrode, whereas Ag/AgCl and Pt functioned as a reference and counter electrode, respectively. The capacity to examine electrochemical processes on various time scales is the strength of electrochemical impedance spectroscopy. The linear sweep voltammetry (LSV) curves for the different samples for the HER are shown in Fig. 5a. S-$PbBr_2$/NF and B-$PbBr_2$/NF demonstrated significantly better HER activity than $PbBr_2$/NF, as predicted, with a significantly lower onset potential and a higher current density. To be specific, pristine S-$PbBr_2$/NF and B-$PbBr_2$/NF achieved an earlier onset potential of -0.239 V and -0.242 V vs. RHE. Here, S-$PbBr_2$/NF was delivered a current density of 10 mA/cm² at an overpotential of -0.262 V, which is -0.265 V for $PbBr_2$/NF, respectively. A fundamental tool for examining and evaluating the efficacy of electrocatalytic chemical imaging of electrode materials is the tafel slope, which is depicted from LSV data. The kinetic reaction of all electrodes was examined using the tafel plot (Fig. 5b), which revealed that the electrochemical reaction rate and the overpotential of the S-$PbBr_2$ and B-$PbBr_2$ electrodes are strongly correlated. The values obtained for $PbBr_2$/NF, S-$PbBr_2$/NF, and B-$PbBr_2$/NF were 142, 100, and 118 mV/dec, respectively; thus, the obtained value demonstrates the Volmer-Heyrovsky mechanism.

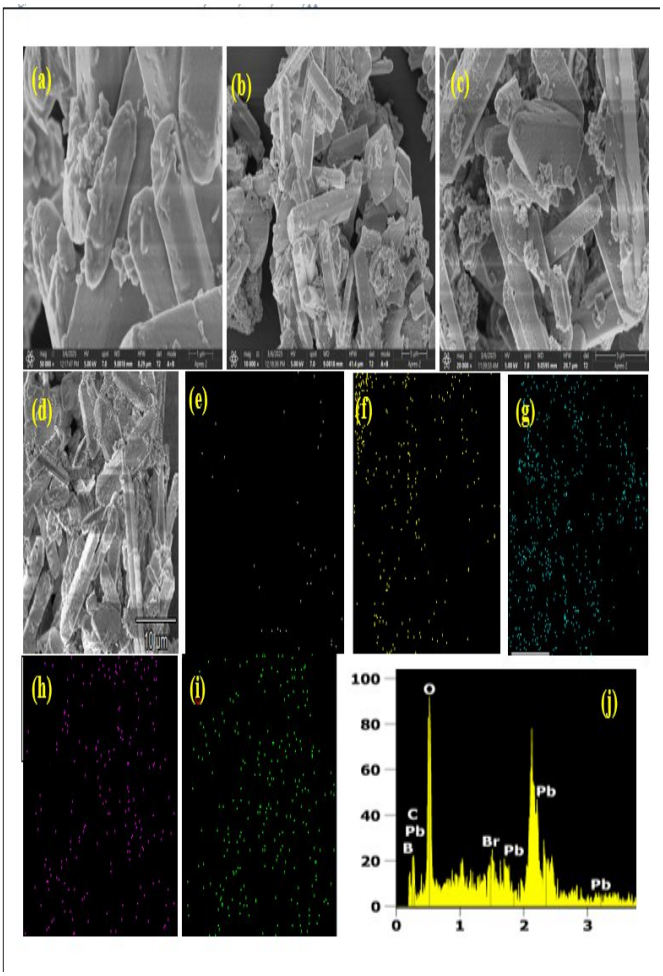

Fig. 3: (a) SEM images of B-$PbBr_2$ at 1 µm, (b) 3 mm, (c) 5mm, (d) elemental mapping of B-$PbBr_2$, (e) B, (f) C, (g) O, (h) Br,(i) Pb elements and (j)EDX analysis

lectrochemical impedance spectroscopy (EIS) results (Figure 7a) show that the $PbBr_2$/NF has a series resistance (Rs) value of 0.6 Ω, while S and B-$PbBr_2$/NF have a value of 0.74 Ω and 0.81 Ω. Compared to pristine $PbBr_2$/NF (14.5 Ω), the charge transfer resistance (Rct) of S-$PbBr_2$ and B-$PbBr_2$ (2.62 Ω and 12.38 Ω) is less because of the high charge-transfer ratio. The EIS data conclusively show that S and B doping improves $PbBr_2$/NF electrocatalytic capabilities for the hydrogen evolution reaction. When S and B are added to $PbBr_2$, it improves electrical conductivity, increases the number of active sites, and increases intrinsic catalytic activity, as seen by the considerable reduction in both series resistance (Rs) and charge transfer resistance (Rct). All of these components work together to improve the efficiency of the HER process, demonstrating that S and B doping is an effective strategy for improving the performance of $PbBr_2$-based electrocatalysts.

The resistance can be decreased and the rate of electron transfer increased by delivering a voltage that is close to the reaction's redox potential. The doping of S and B enhances the $PbBr_2$/NF electrocatalytic capabilities for the hydrogen evolution reaction, according to the EIS data which shows the significant decrease in both series resistance (Rs) and charge transfer resistance (Rct) indicates that increase in electrical conductivity, number of active sites, and boosts intrinsic catalytic activity. Together, these elements increase the HER process's efficiency, suggesting that S and B doping is a useful tactic for enhancing the functionality of $PbBr_2$-based electrocatalysts. The difference between the anodic and cathodic current densities provides the double-layer capacitance (Cdl) of the active electrode, yielding information on a catalyst's electrochemically active surface area. Based on the CV curve, the C_{dl} values for $PbBr_2$/NF, S-$PbBr_2$/NF, and B-$PbBr_2$/NF were 0.15, 0.21, and 10.2 mF/cm^2, respectively (Fig. 7b). By analysing the values of electrochemical analysis, the material is good for the hydrogen evolution reaction.

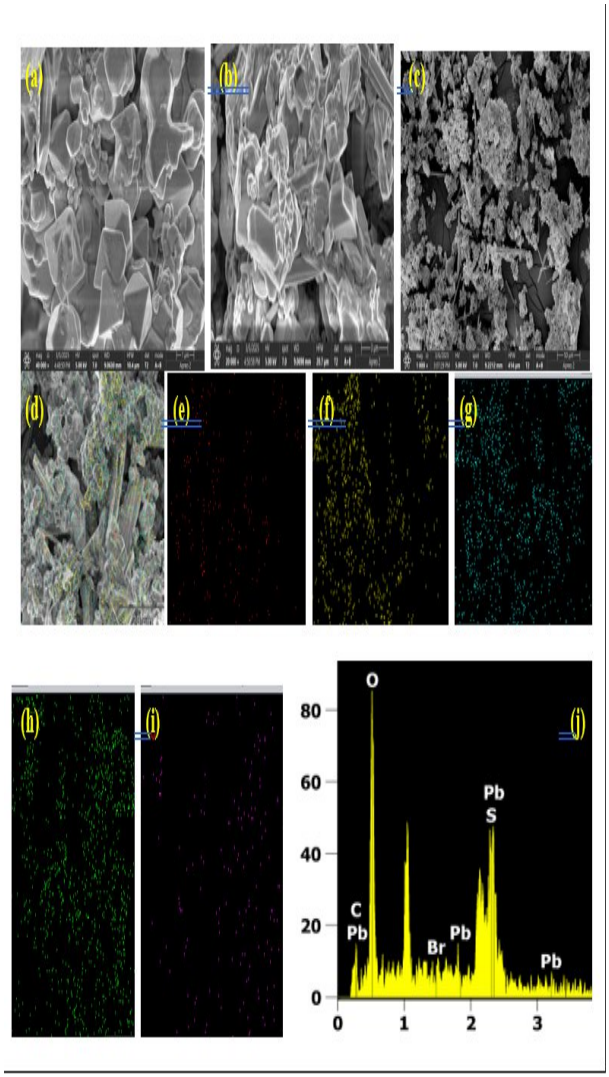

Fig. 4: (a) SEM images of S-PbBr$_2$ at 1µm, (b) 3mm, (c) 50mm, (d) elemental mapping of S-PbBr$_2$, (e) C, (f) O, (g) S, (h) Br,(i)Pb elements and (j)EDX analysis

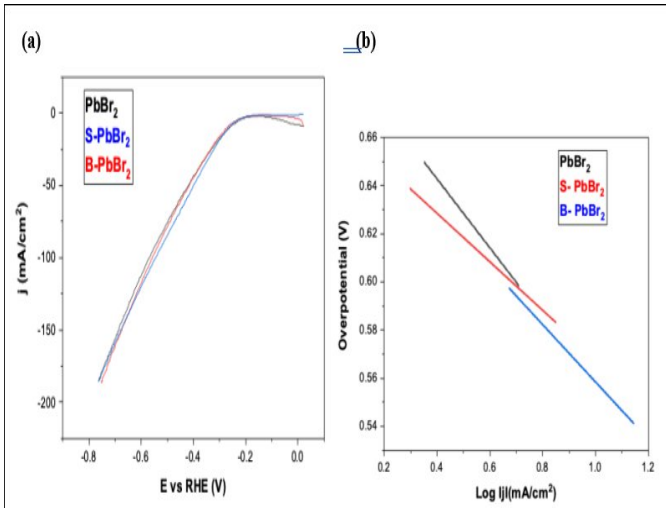

Fig. 5: (a) linear sweep voltammetry curves, (b) Tafel slope

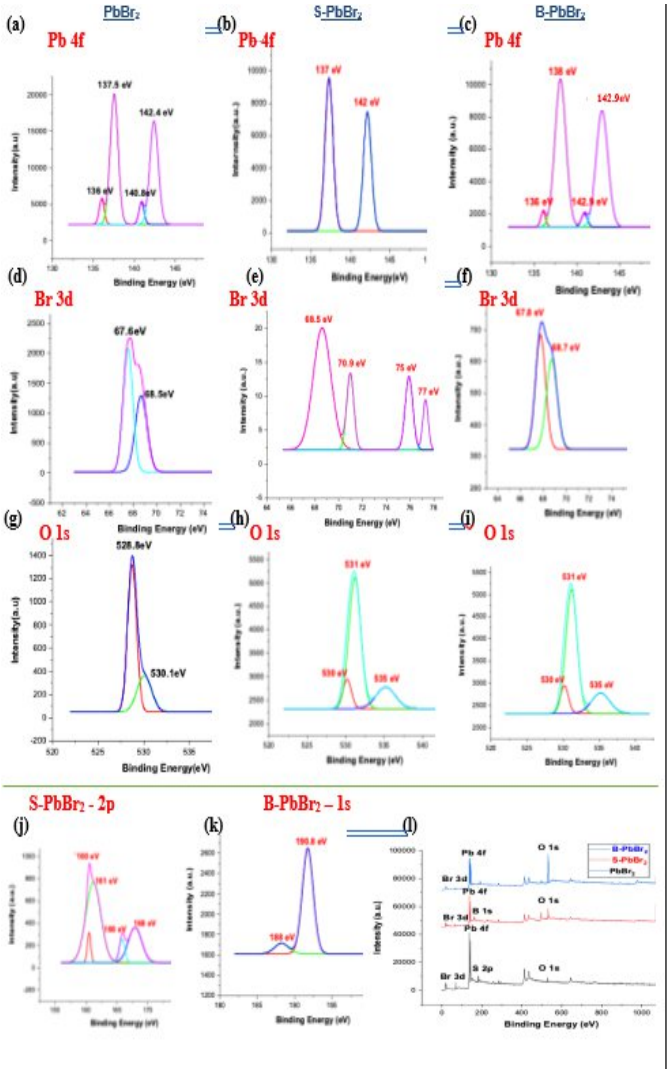

Fig.6: (a-c)Pb4f, (d-f) Br3d, (g-i) O1s spectra of PbBr$_2$, S-PbBr$_2$ and B-PbBr$_2$, (j) 2p state of S-PbBr$_2$, (k) 1s state of S-PbBr$_2$, (l)XPS survey spectra

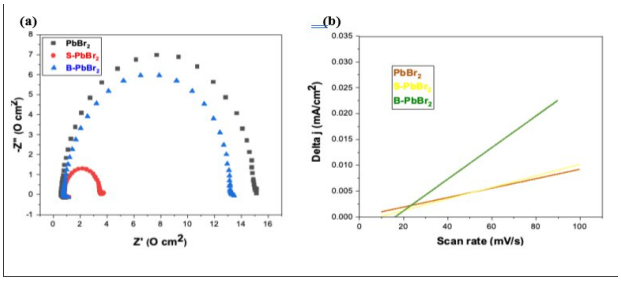

Fig. 7: (a) electrochemical impedance spectroscopy curves, (b) C_{dl} plot

CONCLUSION

In conclusion, a straightforward and successful strategy for utilising the hydrothermal method to create PbBr$_2$/NF, S-PbBr$_2$/NF, and B-PbBr$_2$/NF was proposed and accomplished. In terms of overall alkaline and neutral water splitting methods, the synthesised S-PbBr$_2$/NF and B-PbBr$_2$/NF, as integrated bifunctional electrodes, showed remarkable catalytic characteristics for the HER, attaining 10 mA cm². This was made possible by the optimised composition with favourable conductivity and the well-thought-out 3D hierarchical structure.

Because of its excellent stability, straightforward production process, and strong catalytic activity, B-$PbBr_2$/NF is one of the most promising electrocatalysts for electrochemical water splitting, particularly under neutral circumstances. This study's methodology can be used for various applications such as photocatalysis, metal-air batteries, and supercapacitors, as well as for other mixed transition metal oxides with comparable structures. The synthesised electrocatalyst is a cheap, effective catalyst that performs well in water electrolysis and is a good option for water splitting.

The depreciating prices of renewable energy are a significant factor propelling the potential of hydrogen skyward. Should renewable energy generation become sufficiently economical and widespread, as it could replace fossil fuels in transportation, heating, industrial raw materials, and virtually any application resistant to electrification. Consequently, hydrogen is part of a collection of technologies that synergistically enhance the development of low-carbon energy within the total energy system.

Acknowledgements:

The authors are thankful for the research grant from the UGC section, Veer Narmad South Gujarat University, under the minor research project F.No. UGC/30120/2023. The authors also acknowledge the great support provided by Dr C.K. Sumesh, the Dean of Charotar University of Science and Technology.

Conflict of Interests: The authors declare no conflict of interest.

.

REFERENCES

1. Md Monjur Hossain Bhuiyan, Zahed Siddique, Hydrogen as an alternative fuel: A comprehensive review of challenges and opportunities in production, storage, and transportation, International Journal of Hydrogen Energy, Volume 102, 2025, Pages 1026-1044, ISSN 0360-3199, https://doi.org/10.1016/j.ijhydene.2025.01.033.
2. Prodip K. Das, Frano Barbir, Kui Jiao, Yun Wang, Xianguo Li, Chapter 1 - Fuel cells for transportation—an overview, Woodhead Publishing, 2023, Pages 1-28, ISBN 978032 3994859, https://doi.org/10.1016/B978-0-323-99485-9.00013-7.
3. Salkuyeh Y. K. Saville B. A. MacLean H. L. Techno-Economic Analysis and Life Cycle Assessment of Hydrogen Production from Different Biomass Gasification Processes Int. J. Hydrogen Energy 2018 43 20 9514 9528 . DOI : 10.1016/j.ijhydene.2018.04.024
4. Shahabuddin M. Brooks G. Rhamdhani M. A. Decarbonisation and Hydrogen Integration of Steel Industries: Recent Development, Challenges and Technoeconomic Analysis J. Clean. Prod. 2023 395 136391 . DOI: 10.1016/j .jcle pro.2023.136391
5. Md Kashif Gohar Deshmukh, Mohd Sameeroddin, Daud Abdul, Mohammed Abdul Sattar, Renewable energy in the 21st century: A review, Materials Today: Proceedings, Volume 80, Part 3, 2023, Pages 1756-1759, ISSN 2214-7853, https://doi.org/10.1016/j.matpr.2021.05.501.
6. Tze-Zhang Ang, Mohamed Salem, Mohamad Kamarol, Himadry Shekhar Das, Mohammad Alhuyi Nazari, Natarajan Prabaharan, A comprehensive study of renewable energy sources: Classifications, challenges and suggestions, Energy Strategy Reviews, Volume 43, 2022, 100939, ISSN 2211-467X, https://doi.org/1 0.1016/j.esr.2022.100939.
7. Solanki, Drashti & Shah, Manan & Prajapati, Mitul. (2025). The role of geothermal and wind energy in hydrogen production: towards a carbon-free future. Carbon Neutral Systems. 1. 10.1007/s44438-025-00008-w.
8. Meiling Yue, Hugo Lambert, Elodie Pahon, Robin Roche, Samir Jemei, Daniel Hissel, Hydrogen energy systems: A critical review of technologies, applications, trends and challenges, Renewable and Sustainable Energy Reviews, Volume 146, 2021, 111180, ISSN 1364-0321, https://doi.org/10.1016/j.rser.2021.111180.
9. Kurc, B.; Gross, X.; Szymlet, N.; Rymaniak, Ł.; Woźniak, K.; Pigłowska, M. Hydrogen-Powered Vehicles: A Paradigm Shift in Sustainable Transportation. *Energies* **2024**, *17*, 4768. https://doi.org/10.3390/en17194768
10. Zekai Şen, Solar energy in progress and future research trends, Progress in Energy and Combustion Science, Volume 30, Issue 4, 2004, Pages 367-416, ISSN 0360-1285, https://doi.org/10.1016/j.pecs.2004.02.004.
11. IEA (2019), The Future of Hydrogen, IEA, Paris https://www.iea.org/reports/the-future-of-hydrogen, Licence: CC BY 4.0
12. Zhang J, He J, ang L.; Gan, Z. *Molecules* **2020**, *25*, 1151. https://doi.org/10.3390/molecules25051151
13. https://iea.blob.core.windows.net/assets/9e3a349 3 - b 9 a 6 - 4 b 7 d - b 4 9 9 - 7ca48e357561/The_Future_of_Hydrogen.pdf
14. Shuang Liang, Mingyue Zhang, Gill M. Biesold, Woosung Choi, Yanjie He, Zili Li, Dingfeng Shen, Zhiqun Lin. Advanced Materials. https://doi.org/10.1002/adma.202005888 Volume33, Issue50
15. Onno van der Heijden, Sunghak Park, Rafaël E. Vos, Jordy J. J. Eggebeen, Marc T.M. Koper. ACS Energy Lett. 2024, 9, 4, 1871–1879. https://doi.org/10.1021/acsenergylett.4c00266

.